Sphingomyelin-Cholesterol Domains in Phospholipid Membranes: Atomistic Simulation

Sagar A. Pandit,* S. Vasudevan,* S. W. Chiu,† R. Jay Mashl,† Eric Jakobsson,§ and H. L. Scott*
*Department of Biological, Chemical, and Physical Sciences, Illinois Institute of Technology, Chicago, Illinois 60616; and †Department of Molecular and Integrative Physiology, Department of Biochemistry, University of Illinois at Urbana-Champaign Programs in Biophysics, Neuroscience, and Bioengineering, National Center for Supercomputing Applications, and Beckman Institute, University of Illinois, Urbana, Illinois 61801

ABSTRACT We have carried out an atomic-level molecular dynamics simulation of a system of nanoscopic size containing a domain of 18:0 sphingomyelin and cholesterol embedded in a fully hydrated dioleylposphatidylcholine (DOPC) bilayer. To analyze the interaction between the domain and the surrounding phospholipid, we calculate order parameters and area per molecule as a function of molecule type and proximity to the domain. We propose an algorithm based on Voronoi tessellation for the calculation of the area per molecule of various constituents in this ternary mixture. The calculated areas per sphingomyelin and cholesterol are in agreement with previous simulations. The simulation reveals that the presence of the liquid-ordered domain changes the packing properties of DOPC bilayer at a distance as large as ~8 nm. We calculate electron density profiles and also calculate the difference in the thickness between the domain and the surrounding DOPC bilayer. The calculated difference in thickness is consistent with data obtained in atomic force microscopy experiments.

INTRODUCTION

There is a rapidly growing body of evidence that sphingolipids and cholesterol aggregate in nanometer-sized domains in membranes to form ''functional rafts'' (Simons and Ikonen, 1997; Reitveld and Simons, 1998; Pralle et al., 2000; Jacobson and Dietrich, 1999). For a recent review on rafts, see Edidin (2003). Rafts have been identified as important membrane structural components in signal transduction (Manes et al., 1999; Aman and Ravichandran, 2001; Xavier et al., 1998; Kawabuchi et al., 2000), protein transport (Rozelle et al., 2000; Cheong et al., 1999; Viola et al., 1999), and sorting of membrane components (Manie et al., 2000; Harder et al., 1998; Sönnichsen et al., 2000; Zerial and McBride, 2001). There is also evidence for rafts functioning as sites for the binding and transport into the cell of several pathogens and toxins, including the human immunodeficiency virus 1 (HIV-1) and the prion protein PrP^{sc} (Fantini et al., 2002). In a study of the lateral organization of the plasma membrane of C3H 10T1/2 murine fibroblasts using single-particle tracking, Dietrich et al. (2002) find evidence for nanoscopic domains with lifetimes on the order of tens of seconds.

Due to the complex composition of biological membranes, it is necessary to consider model systems to isolate and characterize the interactions responsible for the formation, stability, size, and mobility of domains. To this end, model systems consisting of binary and ternary lipid mixtures have been under intensive investigation in many laboratories for many years. For reviews on the subject, see Lee (1977) and Silvius (2003). The most striking visual evidence for domain formation comes from fluorescence microscopy studies of mixed phospholipid/cholesterol (Radhakrishnan and McConnell, 1999b,a; Slotte, 1995; Dietrich et al., 2001b) and sphingolipid/cholesterol monolayers (Radhakrishnan et al., 2001; Mattjus and Slotte, 1996). At low surface pressure, and over a variety of cholesterol/lipid concentrations, micrometer-sized domains rich in cholesterol appear and coexist with cholesterol-poor domains. By analysis of the coexistence of domains as a function of temperature and pressure, phase diagrams for mixed monolayer films have been measured (Radhakrishnan and McConnell, 1999b,a; Radhakrishnan et al., 2001; Mattjus and Slotte, 1996).

Stable domains rich in cholesterol and phospholipids also form spontaneously in bilayer vesicles (Dietrich et al., 2001a; Veatch and Keller, 2002; Korlach et al., 1999). At this time, a detailed understanding of the structure of the domains and the mechanisms that control their size, stability, and interactions with other parts of the membrane is lacking for both monolayers and bilayers. In an effort to measure atomic level properties of domains, solid-state NMR has been used to study interactions of cholesterol with bovine brain sphingomyelin (Guo et al., 2002), and a wide variety of biological and model phospholipid-sphingolipid-cholesterol mixtures (Aussenac et al., 2003). On NMR timescales, differences in interaction of cholesterol with phospholipids and sphingolipids are found to be small. In a 1:1:1 mixture of palmitoyloleyl phosphatidylcholine, brain sphingomyelin, and cholesterol, NMR data suggest rapid exchange of cholesterol between two domains of different dynamics (Aussenac et al., 2003), calling into question the existence of stable nanoscopic domains in this system. X-ray scattering and

Submitted February 24, 2004, and accepted for publication May 21, 2004.

Address reprint requests to H. L. Scott, E-mail: scotth@iit.edu.

S. Vasudevan's present address is Dept. of Biochemistry and Molecular Biology, School of Medicine, Southern Illinois University, Carbondale, IL 62901.

0006-3495/04/08/1092/09 $2.00

doi: 10.1529/biophysj.104.041939

calorimetry studies have been carried out by Gandhavadi et al. (2002) and have established some of the structural and thermal properties of sphingomyelin bilayers and their interactions with cholesterol and with unsaturated phospholipids.

Atomic force microscopy has recently been utilized by Rinia et al. (2001) to visualize domains in bilayers consisting of dioleylposphatidylcholine (DOPC), egg sphingomyelin (SM), and varying amounts of cholesterol. Atomic force microscopy (AFM) is able to distinguish domains by height differences in planar bilayers, due to different lipid phases present in the bilayer. Rinia et al. (2001) found 10–100 nm domains in 1:1 binary egg SM-DOPC bilayers at room temperature. Addition of cholesterol to the egg SM-DOPC bilayers in concentrations up to ~15% did not have a strong effect on the size or number of observed domains, or the thickness difference between the domains. At cholesterol concentrations of 25% and higher, the domains became much larger (≈500 nm in size). At 50% cholesterol concentration in 1:1 egg SM-DOPC bilayers, domains were on the order of 10 μm in size. For all cholesterol concentrations <30%, the thickness difference between ordered and disordered domains remained ~0.8 nm. For 30% and 50% cholesterol concentrations, the difference in height was reduced to 0.6 nm and 0.4 nm respectively (Rinia et al., 2001).

To better understand the properties of SM-cholesterol domains on the atomic level of resolution, we have constructed and run a simulation of a single bilayer domain of SM and cholesterol (Chol) of linear size ~10 nm embedded in a surrounding bilayer of phospholipid. We have run the simulation using an unsaturated phospholipid (DOPC) to compare our results with experimental data available for DOPC-SM-Chol systems.

METHODS

Fig. 1 shows the structure of DOPC and SM molecules with the atom labels as the atom types used in this simulation. The system consisted of 1,424 molecules of DOPC, 266 molecules of 18:0 SM, 122 molecules of Chol), and 62,561 water molecules, at a temperature of 20° C . This gave rise to ~12:1:1 proportion of DOPC/SM/Chol in the system. The 2:1 proportion of SM/Chol was used to compare results with our previous simulations of the SM/Chol (2:1) system (Khelashvili and Scott, 2004). A large amount of DOPC was used to reduce the interaction between the domain and its periodic images and to analyze the structure and stability of a nanodomain of SM-Chol, which has a disordered phospholipid boundary. Since we desire to simulate a system in which DOPC is in a disordered phase and SM is in an ordered phase, we chose the simulation temperature to be 20°C, which is approximately midway between the phase transition temperatures of DOPC (−1°C) and SM (~40°C). The lipid nanodomain system was generated as follows: An equilibrated bilayer of 266 SM and 122 Chol was solvated with DOPC (previously equilibrated) using the genbox utility of GROMACS 3.0. The generated system had a box size of 25.8 × 25.8 × 7.3 nm. On solvating the SM-Chol system with pre-equilibrated DOPC molecules, it was observed that one of the leaflets had 20 more DOPCs than the other. These extra 20 DOPCs were randomly removed after visual inspection. The system was then energy minimized in vacuo and solvated with SPC water. The final system before equilibration had 1,424 DOPC (712 in each leaflet), 122 Chol, 266 SM, and 62,561 SPC water molecules.

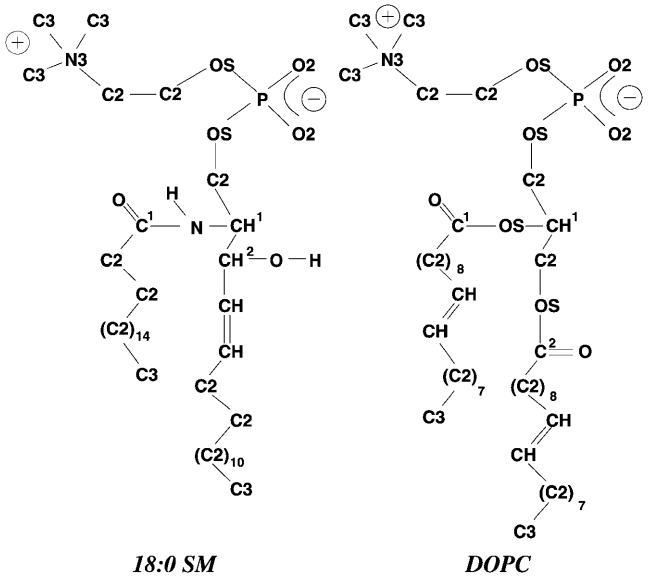

FIGURE 1 Structure of the 18:0 SM and DOPC molecules, with the numbering scheme used in simulation.

The system was energy minimized and then subjected to 4 ps of position restrained molecular dynamics (MD) to relax the solvent. The system was simulated at constant isotropic pressure of 1 atm applied independently to each box dimension. Temperature was maintained by the weak coupling method. The bilayer was equilibrated for 3 ns of MD with a regeneration of velocities from a Maxwellian distribution at 20°C after every 200 ps. This step was performed to ensure proper equilibration of the system. Then a continuous 10 ns trajectory was run without resetting the velocities. Cutoffs of 18 and 20 Å were employed for van der Waals and electrostatics interactions.

Truncation of long-range electrostatic interactions may produce artifacts in simulation (Patra et al., 2003). These artifacts depend on the cutoff range, the use of nonneutral charge groups, and the amount of charge separation in the molecules. In SM-Chol and pure SM systems we found that the area per molecule was sensitive to the cutoff range and that it increased when electrostatic interactions were calculated using Ewald summation (Khelashvili and Scott, 2004; Chiu et al., 2003). Hence, at the end of 10 ns, we started an 8.5 ns simulation in which the long-range electrostatics interactions were calculated using the smooth particle mesh Ewald algorithm (Essmann et al., 1995) with a real space cutoff of 9.5 Å. At the same time, SM force field parameters were also recalculated as described in Chiu et al. (2003).

The time step used for the MD runs was 3 fs, with all bond lengths constrained using the LINCS algorithm (Hess et al., 1997). All MD and energy maximization runs used the GROMACS modeling software suite. (Berendsen et al., 1995; Lindahl et al., 2001) Analysis of the properties of the system was done using a combination of GROMACS utilities and our own analysis programs. Averaging was performed over the last 4 ns of the 8.5 ns trajectory.

Force-field parameters for the phosphocholine polar groups were taken from our dipalmitoylphosphatidylcholine (DPPC) force field (Chiu et al., 1999a). Parameters for the sphingosine chain polar groups were taken from the SM parameter set we developed for the simulation of a large pure 18:0 SM bilayer. (Chiu et al., 2003) Parameters for the hydrocarbon chain atoms were taken from our earlier determination of these quantities by fitting to density and heat of vaporization data (Chiu et al., 1999b).

A test of the stability of the simulation is shown in Fig. 2, where we plot the dimensions of the simulation cell as a function of time over the last 4 ns windows used for averaging. We note that the dimensions of the simulation cell do not show a drift in time.

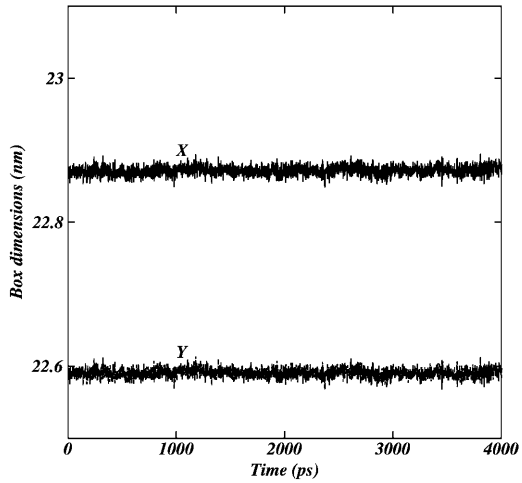

FIGURE 2 *X* and *Y* dimensions of simulation cell as a function of time. Plot shows dimensions of the cell for the trajectory (last 4 ns) that was used for analysis.

RESULTS AND DISCUSSION

Fig. 3 shows snapshots of the simulation system toward the end of the simulation run, viewed from above, below and sidewise, with waters removed for clarity. The domain shape is roughly rectangular, reflecting the shape of the domains at the start of the simulations. This shape was chosen over a circular shape to more fully expose a subset of SM and Chol molecules at the corners to the phospholipids, allowing for observation of potential beginning stages of solvation of individual SM or Chol molecules by the surrounding phospholipid. Examination of the edges of the SM domains in the figure reveals, at a visual level, the difference in the interactions between the SM-Chol domain and the DOPC. Although DOPC itself is highly disordered at 20°C, there is a little visual evidence for mixing of SM and DOPC. However, we see three Chol molecules diffusing into DOPC region. The red circles in the figure show these diffused cholesterol molecules. This suggests a possibility that the cholesterol does not preferentially bind to SM as opposed to DOPC. Recent fluorescence spectroscopy and differential calorimetric studies performed on mixtures of PyrPC, PyrSM, and Chol indicate a lack of specific interaction between SM and Chol (Holopainen et al., 2004). It is suggested by Aussenac et al. (2003) that cholesterol molecules exchange between membrane regions of different dynamics at NMR timescales, presumably between domains with different degree of molecular order. The diffusion of cholesterol into the DOPC region could be a beginning of such exchange. However, a very long time simulation is required to observe this exchange. The side view of the system shows large undulations in the system as one would expect in a system of this size (Lindahl and Edholm, 2000). However, to ensure that the system is not under any stress, we calculated surface tension using the algorithm proposed by Zhang et al. (1995). The calculated surface tension was ~ -4 dyn/cm, which suggested that the system was not under significant stress.

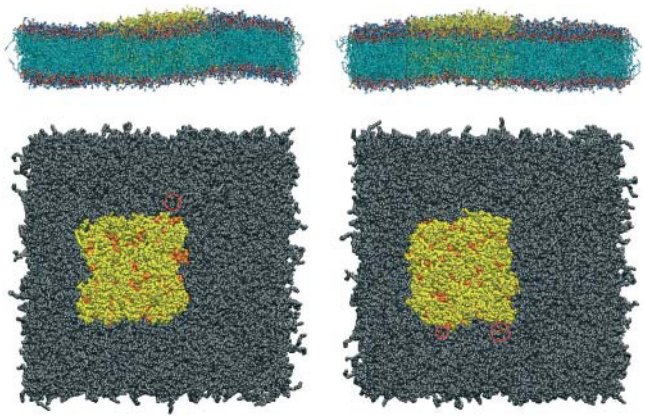

FIGURE 3 Side, top, and bottom snapshots of the simulated system. For clarity, water molecules are removed from the pictures. In top and bottom view, gray corresponds to the liquid crystalline DOPC surrounding, yellow corresponds to SM, and orange corresponds to Chol molecules.

Area per molecule

In the simulation of pure systems, the average area per molecule is generally calculated by taking the ratio of twice the area of the simulation cell to the total number of lipid molecules. However, in mixtures this crude method cannot give areas for each molecular species separately. The problem of calculating the correct area per lipid in cholesterol-DPPC mixtures has been addressed by Hofsäß et al. (2003) and Chiu et al. (2002). Hofsäß et al. resolved this issue by considering the volumes of the constituent molecules and writing the average thickness of the bilayer in terms of the simulation cell volume and area. Chiu et al. performed several simulations with varying concentration of cholesterol and observed a linear relation between the area per molecule and the concentration, from which the area per DPPC and the area per cholesterol could be calculated. However, for a ternary mixture (as we have here) or more complex mixtures of molecules, neither of these methods can be used. Hence, we propose here a novel way of calculating the area per lipid molecule for each molecule type.

We begin by projecting each molecule onto a plane. We then approximate the projected molecule by a two-dimensional polygon of area

$$A_{\text{polygon}} = \frac{1}{2}\sum_{i=0}^{N-1}(x_i y_{i+1} - y_i x_{i+1}), \qquad (1)$$

where N is the number vertices of the polygon and (x_i,y_i) with $i \bmod(N)$ are the coordinates of the vertices of the polygon. A straight forward way of achieving this goal is by taking centers of masses of the molecules and generating a Voronoi tessellation (Jedlovszky et al., 2004; Falck et al., 2004;

Gurtovenko et al., 2003; Patra et al., 2003; Shinoda and Okazaki, 1998). However, for any system with a mixture of molecules of different sizes, this method should overestimate the areas of smaller molecules and underestimate the areas of larger ones. We verified this by calculating the area per molecules in this and another simulation of ternary mixture of DOPC/SM/Chol (S. A. Pandit, E. Jakobsson, and H. L. Scott, unpublished). Hence, we decided to choose certain key atoms on molecules that lie approximately at the interface of hydrophobic and hydrophilic portions of each molecule type. To this end we chose C^1, CH^1, and C^2 for DOPC (See Fig. 1) and C^1, CH^1, and CH^2 for SM. The Chol was represented by the hydroxyl oxygen.

We projected each of these atoms on the $Z = 0$ plane in the simulation box and constructed a Delaunay triangulation of these points. For each of these triangles, we calculated the circumcenters. These circumcenters are the coordinates of the vertices of the Voronoi polygons corresponding to the projected coordinates of the key atoms. The vertices are then sorted to give a consistent orientation for all the polygons. The corresponding atomic polygons are combined to form a molecular polygon. Area analysis was performed on these molecular polygons. Fig. 4 shows a snapshot of the projected CH^1 atoms and molecular polygons.

Since each Voronoi polygon is associated with an individual molecule, we can get the differential average area per molecule for the system. Fig. 5 shows the distributions of the area of polygons corresponding to Chol, SM, and DOPC separately. The areas per Chol, SM, and DOPC calculated using this technique are 29.6 ± 0.3 Å^2, 49.5 ± 0.4 Å^2, and 61.0 ± 0.1 Å^2, respectively. The areas per Chol and SM calculated using the Hofsäß et al. (2003) method for cholesterol-SM binary mixture is ~27.2 Å^2 and ~51.3 Å^2 (Khelashvili and Scott, 2004), respectively. We note that, however, the area per DOPC molecule shows a large deviation from that of previous simulations of pure DOPC bilayers and from experimental data (Nagle and Tristram-Nagle, 2000). This issue will be addressed later in the article. Hence, the method gives correct area per molecule for SM and Chol molecules.

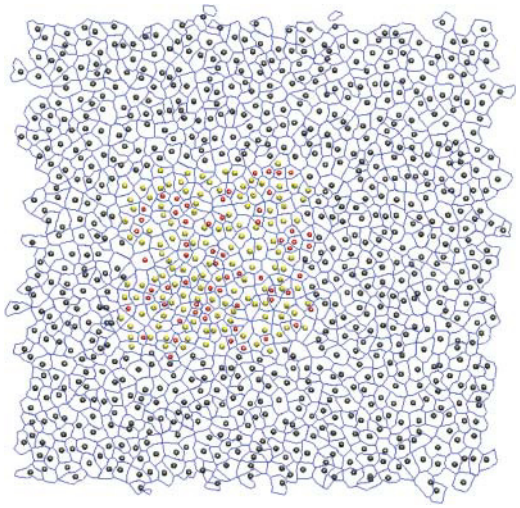

FIGURE 4 A snapshot picture showing the Voronoi tessellation and the key atoms in one leaflet of the system. Color code is the same as Fig. 3.

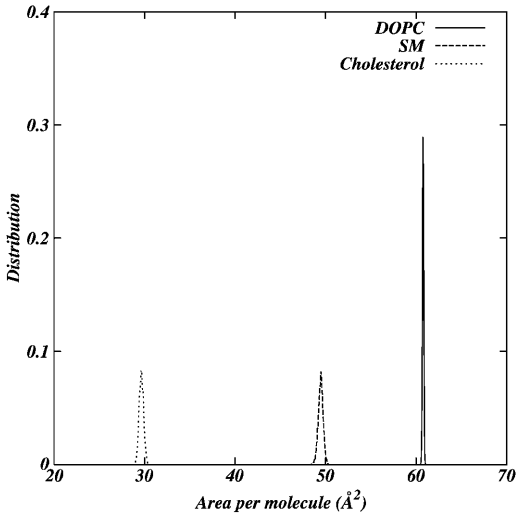

FIGURE 5 Distribution of the area per molecule for each of the constituents of the system.

Effect of the SM-Chol domain on the liquid crystalline phase of DOPC

The presence of a large liquid-ordered SM-Chol domain in a DOPC bilayer affects the structure of the DOPC bilayer. We conjecture that the large deviation in the area per DOPC molecule in our system from the pure DOPC systems is due to the effect of the raft-like domain in the system. To demonstrate the validity of this hypothesis, we calculated the average area per DOPC molecule as a function of the closest distance between a DOPC and an SM molecule in the domain (See Fig. 6). In this context, the distance between two molecules is defined as the shortest distance (with periodic boundaries) between any two atoms of the molecules. As shown in Fig. 6, the presence of the SM-Chol domain affects the area per DOPC for DOPC molecules as far from the domain as 6 nm. The area per DOPC near the domain is ~59 Å^2 and it gradually increases to ~62 Å^2 at a distance of ~6 nm. Fig. 6 shows a dip in the area per DOPC for distances >6 nm. This reduction is an artifact of the shape of the domain. DOPC molecules in this region are 6 nm away from the corner of the domain and appear to be more restricted than the rest. However, we note that the area per DOPC does not reach a value similar to pure DOPC at a distance of 8 nm. Hence, the domain seems to change the organization of DOPC molecules even at large distances. (The Voronoi method, reported here, was used to calculate the area per DOPC in other simulations for the same DOPC

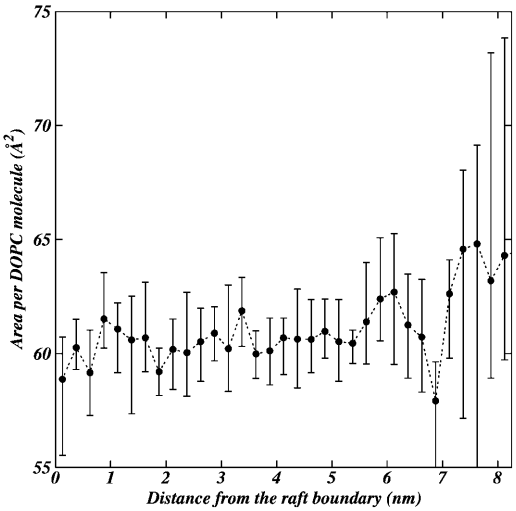

FIGURE 6 Area per DOPC as function of the distance from the SM-Chol domain. In this case, the distance is defined as the shortest distance between any atom of DOPC and any atom of any SM in SM-Chol domain. The error bars are the absolute deviation (not standard deviation) of the area per DOPC averaged over 250 ps time slabs.

force-field parameters (S. A. Pandit, E. Jakobsson, and H. L. Scott, unpublished). The area per DOPC obtained in those simulations was ~70 Å^2, which is in good agreement with the experimental value (Nagle and Tristram-Nagle, 2000). This confirms that the small DOPC area is not an artifact of the DOPC force-field parameters.) At this point we note that the DOPC molecules that are farther than ~6 nm show increase and large variation in the area, but the relative number of such molecules is too small to induce a significant skewness in Fig. 5.

An important structural property of a bilayer is hydrocarbon chain order parameter profile. The ordering of hydrocarbon tails can be determined in NMR experiments by measuring the deuterium order parameters. The order parameter tensor, S, is defined as

$$S_{ab} = \frac{\langle 3\cos(\theta_a)\cos(\theta_b) - \delta_{ab}\rangle}{2} \quad a,b = x,y,z, \qquad (2)$$

where θ_a is the angle made by ath molecular axis with the bilayer normal and δ_{ab} is the Kronecker delta, and can also be calculated in the simulation. In the simulations the order parameter, S_{CD} can be determined using the following relation (Egberts and Berendsen, 1988):

$$-S_{CD} = \frac{2}{3}S_{xx} + \frac{1}{3}S_{yy}. \qquad (3)$$

To study the effect of the raft-like domain on the DOPC bilayer, we divide DOPC molecules into two categories. If a DOPC molecule is <0.5 nm away from the domain (where distance is again defined in the previous paragraph) then we call it a ''boundary'' DOPC and the rest are ''bulk'' DOPCs. We calculated the hydrocarbon chain order parameters for the boundary and bulk DOPC molecules separately. Fig. 7 shows the deuterium order parameter for all the hydrocarbon chains in the systems. We see that the Sn-1 and Sn-2 chains of boundary DOPC show a distinct increase compared to those for bulk DOPC. This result is consistent with the results in Fig. 6. One would like to study the change in order parameter of DOPC chains as a fine-grained function of the distance from the SM-Chol domain, but due to lack of good statistics, we work with this broad classification into boundary and bulk molecules. Fig. 7 also shows chain order parameters for the acyl and sphingosine chains of SM molecules. The sphingosine chain order parameters are not significantly affected by the presence of SM-DOPC boundary. The acyl chain order parameters show a slight reduction in plateau region near the SM-DOPC boundary, but these changes are not as prominent as the changes in DOPC order parameters.

Thickness of the bilayer

The SM-Chol domain is in a liquid-ordered phase, where the hydrocarbon chains are largely in the all *trans* state. Hence one would expect the bilayer to have a greater thickness in this region. AFM experiments indeed report a greater thickness of the raft-like domains (Rinia et al., 2001). A natural method for calculation of average membrane thickness is the peak-to-peak separation of an electron density profile, as the peaks represent the location of electron-rich phosphocholine groups. Fig. 8 is a plot of the calculated electron density profile for the simulation. We note that, due to large undulations (see Fig. 1) and the biphasic nature of the system, the peaks are asymmetric and rather broad. Hence, a simple comparison of the peak separation with experimental data is not straightforward. The

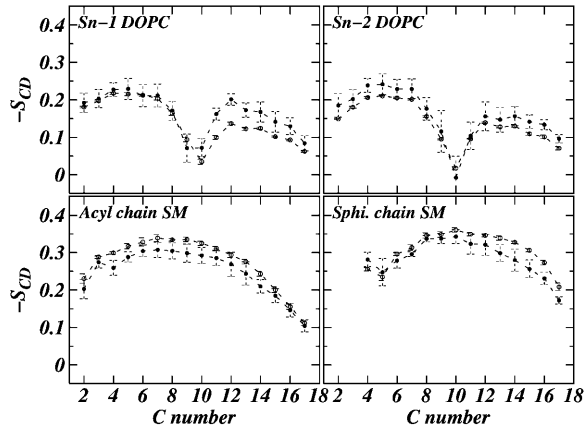

FIGURE 7 Deuterium order parameter for Sn-1, Sn-2 chains of DOPC and acyl, sphingosine chains of SM. The ● shows the order parameters for the molecules that are closer to the domain boundary and ○ shows the order parameters for the molecules that are far from the domain boundary.

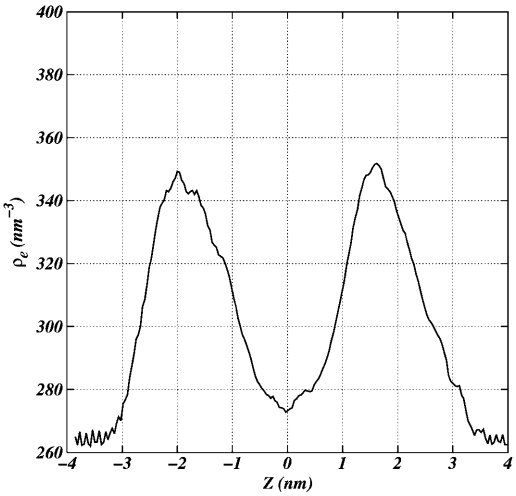

FIGURE 8 Electron density of the simulated system.

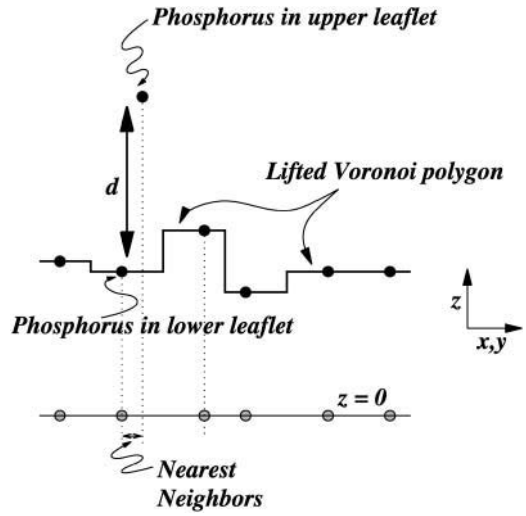

FIGURE 9 Schematic drawing describing the method used to calculate surface to point correlation function.

average peak separation calculated from Fig. 8 is ~36 Å. Since DOPC forms a large portion of the system, the peak separation in electron density is comparable to the peak separations found in previous simulations of pure DOPC bilayers (Mashl et al., 2001). Gandhavadi et al. (2002) find a peak separation of ~43 Å in a DOPC/SM/Chol (1:1:1) mixture. The SM is bovine brain SM in these experiments, and the DOPC fraction is smaller than that in the simulation. These facts account, at least in part, for the difference in peak-to-peak distance between experiment and simulation.

To measure the thickness in reliable way, we first compare the simulation setup with the AFM experimental setup of Rinia et al. (2001). In the experiment, the thickness is measured with respect to a flat surface on which the bilayer is supported. Since we do not have such a flat reference surface, we used an algorithm proposed by Pandit et al. (2003). This algorithm gives a surface-to-point correlation function. The algorithm is described in the schematic drawing in Fig. 9. Here, for each phosphorus in the top leaflet, we first identify the phosphorus in lower leaflet that is approximately below it. This is achieved by

1. Tessellating the lower leaflet into Voronoi polygons.
2. Projecting coordinates of phosphorus from the top leaflet on to this tessellated surface.
3. Identifying the polygon in which the projected coordinates fall. This procedure identifies a trans-bilayer ''neighbor'' for each lipid in the top leaflet.

With this identification, we define the distance of phosphorus in the top leaflet with respect to the surface defined by the phosphorus atoms in the lower leaflet as the normal distance between phosphorus atoms from two leaflets that are ''vertical neighbors'' of each other. This allows us to calculate the densities of phosphorus atoms of DOPC and SM in one leaflet with respect to the surface defined by the phosphorus atoms in the other leaflet.

Fig. 10 shows plots of the densities of phosphorus atoms of SM and DOPC molecules in one leaflet as a function of the distance from the surface defined by the phosphorus atoms from the other leaflet. We note that the SM density shows two peaks. The peak at ~4.5 nm thickness is mainly due to the SM molecules that are on top of DOPC or other SM molecules with lower order parameter. The peak at ~4.8 nm represents SM molecules that are near the center of the domain where SM molecules lie only on top of other SM molecules. The difference in the thickness of SM-Chol domain and the thickness of DOPC calculated from Fig. 10 is ~4.5 ± 0.35 Å for the SM closer to the boundary and ~7.4 ± 0.34 Å for the SM near the center of the raft-like domain. The error estimates of the thickness were calculated by computing the standard deviation of the average thickness

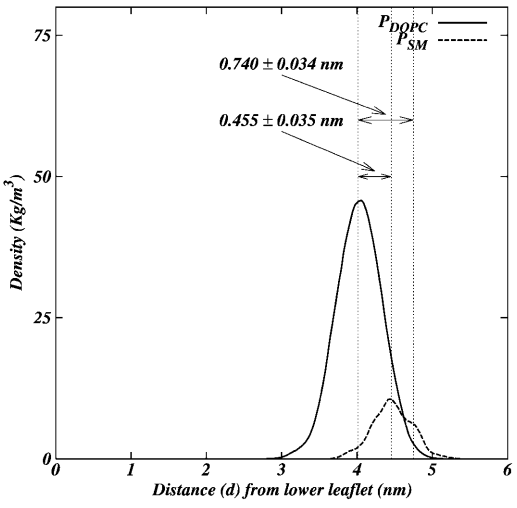

FIGURE 10 Densities of phosphorus atoms of DOPC and SM from one leaflet with respect to the surface defined by the phosphorus atoms from the other leaflet.

calculated over several 250 ps trajectories. Rinia et al. (2001) find this difference in AFM experiments to be ~6 Å.

SUMMARY

We have performed an MD simulation of a nanoscale domain of SM and Chol in a liquid crystalline DOPC bilayer. To the best of our knowledge, this is the largest model membrane simulation using biological lipids to date. The system shows, on a 20 ns timescale, immiscibility of the SM-Chol domain in the surrounding bilayer for the duration of the simulation. However, three cholesterol molecules from the domain diffuse into the surrounding DOPC bilayer, indicating some exchange of cholesterol with the surrounding DOPC.

We proposed a new method of estimating areas per molecule for the constituents of the system. The method is based on Voronoi tessellation using selected ''backbone'' atoms rather than the molecular center of mass. The calculated area per molecule for SM and Chol are in good agreement with the values obtained in previous simulations. The area per DOPC is substantially reduced compared to the area of pure DOPC bilayers from experiment and simulations. We found that the presence of a large liquid-ordered SM-Chol domain affects the packing properties of DOPC bilayer at a distance as large as ~8 nm. Consequently, the order parameters of DOPC hydrocarbon chains show significant difference near and far from the SM-Chol domain.

Due to large undulations in the system, the electron densities are not easily comparable with experiment. Hence, the thickness difference between the domain region and the surrounding region was calculated using the surface-to-point correlation function defined by Pandit et al. (2003). We observed that the SM-Chol domain is ~4.5 Å thicker than the rest of bilayer. This observation is consistent with the AFM experiments performed by Rinia et al. (2001). The simulated system has a much larger relative proportion of DOPC than that used by Rinia et al. The structure of the simulated system, consisting of a single SM-Chol domain surrounded by DOPC, may in fact have a different thickness profile than a purely random DOPC-SM-Chol mixture (Gandhavadi et al., 2002). If the experimental system has domains rich in SM-Chol, then we expect that the comparison of domain constituents with the system used by Rinia et al. should exhibit similar behavior.

A more general issue that is raised by the lowered DOPC molecular area is: how does the presence of a rigid, ordered, object or molecule affect surrounding, otherwise disordered, lipid? At the molecular level, we have used simulations to study relation between the saturated lipid DPPC and Chol (Chiu et al., 2002). In that work we found that, at concentrations ranging from ~12% to ~50% Chol, the system exhibited characteristics of a liquid-ordered phase, with an effective area per DPPC of ~50.7 $Å^2$, which is ~10 $Å^2$ less than the liquid crystalline area per DPPC. Recently, we performed simulations of 18:0 SM and Chol at a proportion of 2:1 (Khelashvili and Scott, 2004). In these simulations, we found that Chol did not appreciably alter the area per SM and the packing behavior of SM at 50°C and 20°C. The difference between the behavior of the SM/Chol mixture and the DPPC/Chol mixture should not be surprising, because in the pure SM systems, the SM molecules have a smaller area and are more ordered than are DPPC molecules in a pure DPPC bilayer at the same temperature. We expect a mixture of DOPC/Chol to behave qualitatively similarly to a DPPC/Chol mixture at the same concentration. Indeed, in earlier simulations of POPC/Chol at ~6% Chol (Chiu et al., 2001), the effect of Chol on POPC was similar to that of DPPC. Hence, the reduction in DOPC area due to presence of a large liquid-ordered domain in the current simulation appears consistent with the behavior seen at a molecular scale in systems consisting of disordered lipids and Chol.

Scherfeld et al. (2003) investigated ternary mixtures of DOPC/DPPC/Chol and DOPC/SM/Chol using confocal fluorescence microscopy, and argued that domain formation in DOPC/DPPC/Chol requires greater concentration of Chol than needed for domain formation in DOPC/SM/Chol mixtures. Their data further suggest a preference of Chol for SM over DPPC. Our simulation cannot directly address this issue. However, comparison of simulations of SM/Chol mixture and DPPC/Chol mixture, discussed above, are consistent with a scenario in which small, but possibly important, differences in the interactions of Chol with SM and DPPC or DOPC exist. In related work, at very high concentration of Chol in DOPC bilayer (50% and 57%), Parker et al. (2004) find evidence, using fluorescent anisotropy and fluorescent resonant energy transfer, for large-scale ordering of Chol molecules, consistent with a ''tiling'' of the bilayer by DOPC/Chol complexes. It is likely that such complexes also form at lower Chol concentrations, as observed in experiments (McConnell and Radhakrishnan, 2003) and simulations (Pandit et al., 2004a; Chiu et al., 2002).

To make more progress on the issue of domain formation, stability, and structure using atomistic simulations, much longer timescales are needed. If times of the order of a few hundred nanoseconds can be sampled, it will be possible to monitor the motions of lipid and cholesterol molecules as they move laterally over 1–2 nm. Although even this scale will not allow the visualization of whole-domain formation, it will sample the initial states of intermolecular aggregation that ultimately must precede domain formation. We are currently running MD simulations of 1:1 DOPC/SM and 1:1:1 DOPC/SM/Chol systems that are sufficiently large (~400 lipids) to allow for multiple intermolecular configurations, but sufficiently small to allow simulations to run for a few tenths of a microsecond.

Supported by National Institutes of Health grant GM54651.

Computer time was provided by the National Center for Supercomputing Applications.

REFERENCES

Aman, M. J., and K. S. Ravichandran. 2001. A requirement for lipid rafts in B cell receptor induced Ca^{2+} flux. *Curr. Biol.* 10:393–396.

Aussenac, F., M. Tavares, and E. J. Dufourc. 2003. Cholesterol dynamics in membranes of raft composition: a molecular point of view from ^{2}H and ^{31}P solid-state NMR. *Biochemistry.* 42:1383–1390.

Berendsen, H., D. van der Spoel, and R. van Drunen. 1995. GROMACS: a message-passing parallel molecular dynamics implementation. *Comput. Phys. Commun.* 91:43–56.

Cheong, K. H., D. Zachetti, E. Schneeberger, and K. Simons. 1999. VIP17/MAL, a lipid raft-associated protein, is involved in apical transport in MDCK cells. *Proc. Natl. Acad. Sci. USA.* 96:6241–6248.

Chiu, S.-W., M. M. Clark, E. Jakobsson, S. Subramaniam, and H. L. Scott. 1999a. Application of a combined Monte Carlo and molecular dynamics method to the simulation of a dipalmitoylphosphatidylcholine lipid bilayer. *J. Comput. Chem.* 20:1153–1164.

Chiu, S.-W., M. M. Clark, E. Jakobsson, S. Subramaniam, and H. L. Scott. 1999b. Optimization of hydrocarbon chain interaction parameters: Application to the simulation of fluid phase lipid bilayers. *J. Phys. Chem. B.* 103:6323–6327.

Chiu, S.-W., E. Jakobsson, R. J. Mashl, and H. L. Scott. 2002. Cholesterol-induced modifications in lipid bilayers: a simulation study. *Biophys. J.* 83:1842–1853.

Chiu, S.-W., E. Jakobsson, and H. L. Scott. 2001. Combined Monte Carlo and molecular dynamics simulation of hydrated lipid-cholesterol lipid bilayers at low cholesterol concentration. *Biophys. J.* 80:1104–1114.

Chiu, S.-W., S. Vasudevan, E. Jakobsson, R. J. Mashl, and H. L. Scott. 2003. Structure of sphingomyelin bilayers: a simulation study. *Biophys. J.* 85:3624–3635.

Dietrich, C., L. A. Bagatolli, Z. N. Volovyk, N. L. Thompson, M. Levi, K. Jacobson, and E. Gratton. 2001a. Lipid rafts in model membranes. *Biophys. J.* 80:1417–1428.

Dietrich, C., Z. N. Volovyk, M. Levi, N. L. Thompson, and K. Jacobson. 2001b. Partitioning of Thy-1, GM1, and cross-linked phospholipids analogs into lipid rafts reconstituted in supported model membrane monolayers. *Proc. Natl. Acad. Sci. USA.* 98:10642–10647.

Dietrich, C., B. Yang, T. Fuiwara, A. Kusumi, and K. Jacobson. 2002. Relationship of lipid rafts to transient confinement zones detected by single particle tracking. *Biophys. J.* 82:244–284.

Edidin, M. 2003. The state of lipid rafts: from model membranes to cells. *Annu. Rev. Biophys. Biomol. Struct.* 32:257–283.

Egberts, E., and H. J. C. Berendsen. 1988. Molecular dynamics simulation of a smectic liquid crystal with atomic detail. *J. Chem. Phys.* 89:3718–3732.

Essmann, U., L. Perera, M. L. Berkowitz, T. Darden, H. Lee, and L. G. Pedersen. 1995. A smooth particle mesh Ewald method. *J. Chem. Phys.* 103:8577–8593.

Falck, E., M. Patra, M. Karttunen, M. T. Hyvönen, and I. Vattulainen. 2004. Lessons of slicing membranes: interplay of packing, free area, and lateral diffusion in phospholipid/cholesterol bilayers. http://www.arxiv.org/abs/cond-mat/0402290.

Fantini, J., N. Garmy, R. Mahfoud, and N. Yahi. 2002. Lipid rafts: structure, function, and role in HIV, Alzheimers, and prion diseases. *Expert Rev. Mol. Med.* 20:1–21.

Gandhavadi, M., D. Allende, A. Vidal, S. Simom, and T. Mcintosh. 2002. Structure, composition, and peptide binding properties of detergent soluble bilayers and detergent resistant rafts. *Biophys. J.* 82:1469–1482.

Guo, W., V. Kurze, T. Huber, N. Afdhal, K. Beyer, and J. A. Hamilton. 2002. A solid state NMR study of phospholipid-cholesterol interactions: sphingomyelin-cholesterol binary systems. *Biophys. J.* 83:1465–1478.

Gurtovenko, A. A., M. Patra, M. Karttunen, and I. Vattulainen. 2003. Cationic DMPC/DMTAP lipid bilayers: molecular dynamics study. http://www.arxiv.org/abs/cond-mat/0312400.

Harder, T., P. Scheiffele, P. Verkade, and K. Simons. 1998. Lipid domain structure of the plasma membrane revealed by patching of membrane components. *J. Cell Biol.* 141:929–942.

Hess, B., H. Bekker, H. J. C. Berendsen, and J. G. E. M. Fraaige. 1997. LINCS: a linear constraint solver for molecular simulations. *J. Comput. Chem.* 18:1463–1472.

Hofsäß, C., E. Lindahl, and O. Edholm. 2003. Molecular dynamics simulations of phospholipid bilayers with cholesterol. *Biophys. J.* 84: 2192–2206.

Holopainen, J. M., A. J. Metso, J.-P. Mattila, A. Jutila, and P. K. J. Kinnunen. 2004. Evidence for the lack of specific interaction between cholesterol and sphingomyelin. *Biophys. J.* 86:1510–1520.

Jacobson, K., and C. Dietrich. 1999. Looking at lipid rafts? *Trends Cell Biol.* 9:87–91.

Jedlovszky, P., N. N. Medvedev, and M. Mezei. 2004. Effect of cholesterol on the properties of phospholipid membranes. 3. Local lateral structure. *J. Phys. Chem. B.* 108:465–472.

Kawabuchi, M., Y. Satomi, T. Takao, Y. Shimonishi, S. Nada, K. Nagai, A. Tarakhovsky, and M. Okada. 2000. Transmembrane phosphoprotein cbp regulates the activities of scr-family tyrosine kinases. *Nature.* 404:999–1002.

Khelashvili, G. A., and H. L. Scott. 2004. Combined Monte Carlo and molecular dynamics simulation of hydrated sphingomyelin-cholesterol lipid bilayers. *J. Chem. Phys.* 120:9841–9847.

Korlach, J., P. Schwille, W. W. Webb, and G. W. Feigenson. 1999. Characterization of lipid bilayer phases by confocal microscopy and fluorescence correlation spectroscopy. *Proc. Natl. Acad. Sci. USA.* 96: 8461–8466.

Lee, A. G. 1977. Lipid phase transitions and phase diagrams II. Mixtures involving lipids. *Biochim. Biophys. Acta.* 472:285–344.

Lindahl, E., and O. Edholm. 2000. Mesoscopic undulations and thickness fluctuations in lipid bilayers from molecular dynamics simulations. *Biophys. J.* 79:426–433.

Lindahl, E., B. Hess, and D. van der Spoel. 2001. GROMACS 3.0: A package for molecular simulation and trajectory analysis. *J. Mol. Model.* 7:306–317.

Manes, S., E. Mira, C. Gomez-Moulton, R. A. Lacalle, P. Keller, J. P. Labrador, and A. C. Martinez. 1999. Membrane raft microdomains mediate front-rear polarity in migrating cells. *EMBO J.* 18:6211–6220.

Manie, S. N., S. Debreyne, S. Vincent, and D. Gerlier. 2000. Measles virus structural components are enriched into lipid raft microdomains: a potential cellular location for virus assembly. *J. Virol.* 74:305–311.

Mashl, R. J., H. L. Scott, S. Subramaniam, and E. Jakobsson. 2001. Molecular simulation of dioleoylphosphatidylcholine lipid bilayers at differing levels of hydration. *Biophys. J.* 81:3005–3015.

Mattjus, P., and P. Slotte. 1996. Does cholesterol discriminate between sphingomelin and phosphatidylcholine in mixed monolayers containing both phospholipids? *Chem. Phys. Lipids.* 81:69–80.

McConnell, H. M., and A. Radhakrishnan. 2003. Condensed complexes of cholesterol and phospholipids. *Biochim. Biophys. Acta.* 1610:159–173.

Nagle, J. F., and S. Tristram-Nagle. 2000. Structure of lipid bilayers. *Biochim. Biophys. Acta.* 1469:159–195.

Pandit, S. A., D. Bostick, and M. L. Berkowitz. 2003. An algorithm to describe molecular scale rugged surfaces and its application to the study of a water/lipid bilayer interface. *J. Chem. Phys.* 119:2199–2205.

Pandit, S. A., D. L. Bostick, and M. L. Berkowitz. 2004a. Complexation of phosphatidylcholine lipids with cholesterol. *Biophys. J.* 86:1345–1356.

Parker, A., K. Miles, K. H. Cheng, and J. Huang. 2004. Lateral distribution of cholesterol in dioleylposphatidylcholine lipid bilayers: cholesterol-phospholipid interactions at high cholesterol limit. *Biophys. J.* 86:1532–1544.

Patra, M., M. Karttunen, M. Hyvönen, E. Falck, P. Lindqvist, and I. Vattulainen. 2003. Molecular dynamics simulations of lipid bilayers: major artifacts due to truncating electrostatic interactions. *Biophys. J.* 84:3636–3645.

Pralle, A., P. Keller, E. L. Florin, K. Simone, and J. H. K. Horber. 2000. Sphingolipid-cholesterol rafts diffuse as small entities in the plasma membrane of mammalian cells. *J. Cell. Biol.* 148:997–1007.

Radhakrishnan, A., X.-M. Li, R. E. Brown, and H. M. McConnell. 2001. Stoichiometry of cholesterol-sphingomyelin condensed complexes in monolayers. *Biochim. Biophys. Acta.* 1511:1–6.

Radhakrishnan, A., and H. M. McConnell. 1999a. Cholesterol-phospholipid complexes in membranes. *J. Am. Chem. Soc.* 121:486–487.

Radhakrishnan, A., and H. M. McConnell. 1999b. Condensed complexes of cholesterol and phospholipid. *Biophys. J.* 77:1507–1517.

Reitveld, A., and K. Simons. 1998. The differential miscibility of lipids as the basis for the formation of functional membrane rafts. *Biochim. Biophys. Acta.* 1376:467–479.

Rinia, H. A., M. M. E. Snel, J. P. J. M. van der Eerden, and B. de Kruijff. 2001. Visualizing detergent resistant domains in model membranes with atomic force microscopy. *FEBS Lett.* 501:92–96.

Rozelle, A. L., L. M. Machesky, M. Yamamoto, M. H. Driessens, R. H. Insall, M. G. Roth, K. Luby-Phelps, G. Marriott, A. Hall, and H. L. Yin. 2000. Phosphatidylinositol 4,5-biphosphate induces actin-based movement of raft-enriched vesicles through WASP-Arp2/3. *Curr. Biol.* 6:311–320.

Scherfeld, D., N. Kahya, and P. Schwille. 2003. Lipid dynamics and domain formation in model membranes composed of ternary mixtures of unsaturated and saturated phosphatidylcholines and cholesterol. *Biophys. J.* 85:3758–3768.

Shinoda, W., and S. Okazaki. 1998. A Voronoi analysis of lipid area fluctuation in a bilayer. *J. Chem. Phys.* 109:1517–1521.

Silvius, J. R. 2003. Role of cholesterol in lipid raft formation: lessons from lipid model systems. *Biochim. Biophys. Acta.* 1610:174–183.

Simons, K., and E. Ikonen. 1997. Functional rafts in cell membranes. *Nature.* 387:569–572.

Slotte, P. 1995. Lateral domain heterogeneity in cholesterol/phosphatidylcholine monolayers as a function of cholesterol concentration and phosphatidylcholine chain length. *Biochim. Biophys. Acta.* 1238:118–126.

Sönnichsen, B., S. de Renzis, E. Nielsen, J. Reitdorf, and M. Zerial. 2000. Distinct membrane domains on endosomes in the recycling pathway visualized by multicolor imaging of Rab4, Rab5, and Rab1. *J. Cell Biol.* 149:901–914.

Veatch, S. L., and S. L. Keller. 2002. Organization in lipid membranes containing cholesterol. Phys. Rev. Lett. 89:268101–1—268101–4.

Viola, A., S. Schroeder, Y. Sakakibara, and A. Lanzavecchia. 1999. T lymphocyte costimulation mediated by reorganization of membrane microdomains. *Science.* 283:680–682.

Xavier, R., T. Brennan, Q. Li, C. McCormack, and B. Seed. 1998. Membrane compartmentation is required for efficient T cell activation. *Immunity.* 6:723–732.

Zerial, M., and H. McBride. 2001. Rab proteins as membrane organizers. *Nat. Rev. Mol. Cell Biol.* 2:107–117.

Zhang, Y., S. E. Feller, B. R. Brooks, and R. W. Pastor. 1995. Computer simulation of liquid/liquid interface. I. theiry and application to octane/water. *J. Chem. Phys.* 103:10252–10266.